SUPPLEMENTAL FIGURE LEGENDS

Figure S1. *C. elegans* ESCRT-II and Vps20 exhibit similar hydrodynamic properties to their human counterparts and do not sense elevated membrane curvature individually. (A) Graphical representation of the results from dynamic light scattering measurements, which define the sizes of liposomes that form following extrusion through membranes harboring 30 nm (red line) and 200 nm (blue line) pores (n=2 independent experiments). (B) Purified *C. elegans* ESCRT-II (top) and Vps20 (bottom) were fractionated over glycerol gradients (10-30%), and their sedimentation values were calculated based on the mobility of characterized standards separated on parallel gradients (n=3). (C) Sequence alignments between *C. elegans* and human ESCRT-II and Vps20 proteins. Identical (red) and similar (blue) residues are highlighted. *C. elegans* Vps25 is encoded by W02A11.2, Vps22 by C27F2.5, Vps36 by F17C11.8, Vps20 by Y65B4A.3, and Vps32 (essential isoform) by C56C10.3. (D) Schematic representation of a co-flotation assay used to determine whether proteins associate with liposomes.

Figure S2. Membrane binding of ESCRT-II/Vps20 increases as the square of the membrane curvature and association of Vps20 with ESCRT-II lowers the affinity of ESCRT-II for flat membranes. (A) BODIPY-FL-labeled Vps20 (right) and ESCRT-II were mixed and incubated with immobilized liposomes containing Rhodamine-PE (left) on a coverslip prior to imaging using confocal microscopy. A merged panel showing the localization of Vps20 (green) relative to Rhodamine-PE liposomes (red) is shown below. Bar, 2 μm. (B) The fluorescence intensity of individual liposomes was measured. Rhodamine intensity was plotted against the fluorescence intensity of BODIPY-FL divided by the fluorescence intensity of rhodamine. Data are representative of at least 3 independent experiments. A best fit curve was

generated that is described by the following equation: $y = kx^{-0.993}$, where k is a constant (R^2 value = 0.95). (C) BODIPY-FL-labeled Vps20 (right) was incubated with immobilized liposomes containing Rhodamine-PE (left) on a coverslip prior to imaging using confocal microscopy. A merged panel showing the localization of Vps20 (green) relative to Rhodamine-PE liposomes (red) is shown below. Bar, 2 μm. (D) Representative AFM image of a bilayer formed in the absence of proteins. Arrows highlight gaps in the bilayer, where the exposed mica surface can be visualized. A shade-height scale bar is shown on the right. White scale bar, 500 nm. (E) A schematic diagram illustrating the likely topology of the membrane at the edges of supported lipid bilayers. The typical height of a bilayer formed on a mica surface is approximately 4 nm, although the measured thickness is usually less because of partial penetration of the bilayer by the probe. (F) Using AFM, the total number of ESCRT-II particles bound to the bilayer was counted in the presence of varying concentrations of Vps20 (0-450 nM). In each case, the concentration of ESCRT-II used remained constant (150 nM). Each experiment was conducted at least 2 times, and an area of at least 450 μm^2 was analyzed for each replicate. (G) A representative AFM image of a bilayer composed of phosphatidylcholine (55%), phosphatidylethanolamine (30%), and phosphatidylserine (15%) assembled in the presence of ESCRT-II (150 nM) and Vps20 (450 nM). Arrows highlight ESCRT-II/Vps20 particles bound to the edges of bilayers, which is independent of phosphoinositides. A shade-height scale bar is shown on the right. White scale bar, 500 nm.

Figure S3. ESCRT-III filaments form specifically on highly curved membranes. (A) Vps32 initially purified using nickel affinity chromatography was subjected to size exclusion chromatography, and the peak fractions eluted were separated by SDS-PAGE and stained using

Coomassie blue (top). For comparison, the elution profile of carbonic anhydrase, a globular, monomeric protein of a similar molecular weight is shown (bottom). A Stokes radius for Vps32 was calculated based on the elution profile of characterized standards (n=3). (B) Purified Vps32 was fractionated over a glycerol gradient (10-30%), and its sedimentation value was calculated based on the mobility of characterized standards separated on parallel gradients (n=3). For comparison, the fractionation profile of carbonic anhydrase is shown (bottom). (C) A representative AFM image of a bilayer formed in the presence of Vps20 (150 nM). A shade-height bar is shown on the right. White scale bar, 250 nm. (D) A representative AFM image of a bilayer formed in the presence of Vps32 (450 nM). A shade-height bar is shown on the right. White scale bar, 250 nm. (E) A schematic diagram showing that proteins bound to the edges of bilayers are not visible unless additional force is applied by the AFM tip to compress the bilayer. Apparent heights of the bilayer are shown. (F) The top panel shows a representative AFM image of a bilayer formed in the presence of ESCRT-II (100 nM), Vps20 (150 nM), and Vps32 (450 nM). A shade-height bar is shown on the right. White scale bar, 100 nm. The bottom panel is a schematic representation of the top panel, highlighting the spatial distribution of ESCRT-II (blue), Vps20 (green), and Vps32 (yellow). The ESCRT-II/Vps20 complex (encircled in white) is also shown. (G) Additional representative AFM images of bilayers formed as in F at high magnification. Arrows highlight ESCRT-II/Vps20 nucleation complexes. A shade-height bar is shown on the right. White scale bar, 50 nm. (H) Frequency distribution of molecular volumes for Vps32 monomers within filaments bound to the edges of lipid bilayers. More than 20 filaments were analyzed in 3 independent experiments.

Figure S4. ESCRT-III assembly promotes membrane remodeling and bilayer sealing on a mica surface. Using AFM, the surface area of mica that remained exposed following SLB assembly was calculated over a region greater than 2.25 μm^2 at different time intervals, both in the presence (blue) and absence (red) of ESCRT-II (150 nM), Vps20 (150 nM), and Vps32 (450 nM). Four independent experiments are shown as a percent change in the area of exposed mica over time.

SUPPLEMENTAL MOVIE LEGENDS

Movie S1. GUV membrane dynamics. GUVs containing rhodamine-labeled PE were imaged in a protein-free suspension (without compression) using swept field confocal optics. Images were acquired every 100 msec in resonant scan mode. Spontaneous deformations in the limiting membrane of the GUV are apparent. Additionally, the spontaneous formation of a vesicle that buds into the lumen of the GUV can be observed. The diameter of the GUV is approximately 12.3 μm.

Movie S2. Spontaneous vesicle formation within GUVs. GUVs containing rhodamine-labeled PE were imaged in a protein-free suspension (without compression) using swept field confocal optics. Images were acquired every 100 msec in resonant scan mode. Multiple spontaneous vesicles that bud into the GUV lumen can be observed. The diameter of the GUV is approximately 3.1 μm.

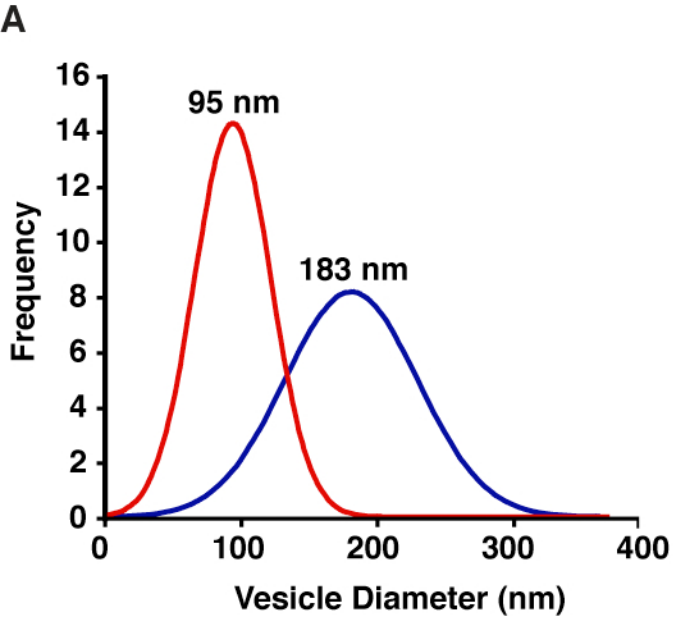

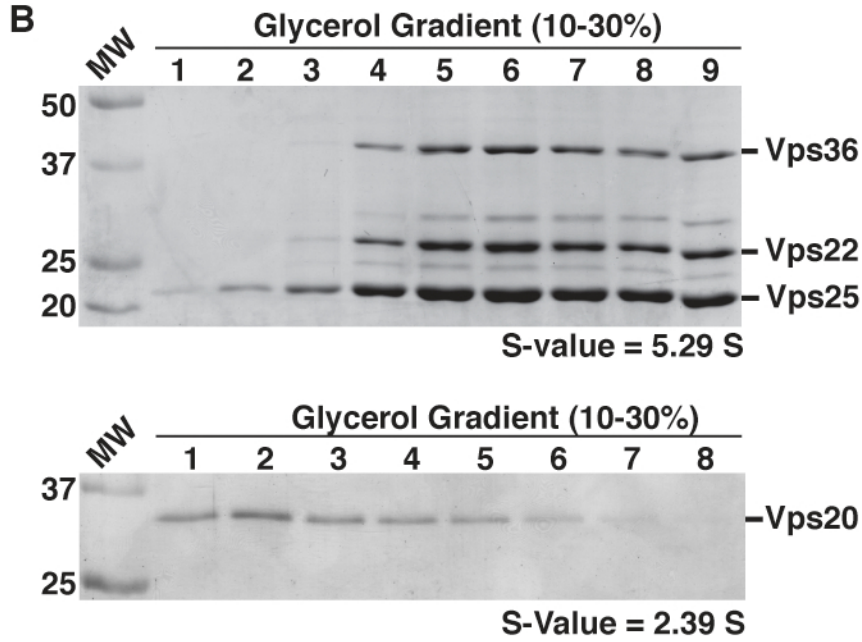

C

Vps25

```
C. elegans 8   ASAFKWPWQYDFPPFFTIQKSLNTKDKQLEAWARLVIDYAQHNKIYSLDIAEATTSELFN  67
H. sapiens 2   AMSFEWPWQYRFPPFFTLQPNVDTRQKQLAAWCSLVLSFCRLHKQSSMTVMEAQESPLFN  61

C. elegans 68  NQKLNRRLSTDGVNTVLQYLEQKKLIEFTDNGRTRFHIFWRRPDVWANMIYQWAVENAFI  127
H. sapiens 62  NVKLQRKLPVESIQIVLEELRKKGNLEWLDKSKSSFLIMWRRPEEWGKLIYQWVSRSGQN  121

C. elegans 128 NTPLTLYEITHGDDTTNESFHNLEREILMKALTCLEEQRRAQLMNIGGDNEGVKF      182
H. sapiens 122 NSVFTLYELTNGEDTEDEEFHGLDEATLLRALQALQQEHKAEIITV-SDGRGVKF      175
```

Vps22

```
C. elegans 4   RRRIGVAAIQKKQETANKFAAKGDQMAGEQLVQFSQQLEQLSAGLEMFAQRHRDEIKKNS  63
H. sapiens 3   RRGVGAGAIAKKKLAEAKYKERGTVLAEDQLAQMSKQLDMFKTNLEEFASKHKQEIRKNP  62

C. elegans 64  QFRRHFQEMCASVGVDPLASSKGFWAKALGFGDFYYELGIQIVEICLSTTHINGGIMTVE  123
H. sapiens 63  EFRVQFQDMCATIGVDPLASGKGFWSEMLGVGDFYYELGVQIIEVCLALKHRNGGLITLE  122

C. elegans 124 EIRNRLMRTRSRTRKDTISTDDILRAVDKLKVLGNGFELVPLGGGRFLVQSVPGELSMDH  183
H. sapiens 123 ELHQQVLKGRGKFAQD-VSQDDLIRAIKKLKALGTGFGIIPV-GGTYLIQSVPAELNMDH  180

C. elegans 184 SRVLQLAEDAAYVTKELIIDKLRWDEARASSALEHLVKEGLAWTDEQASDTTQYWFPSLF  243
H. sapiens 181 TVVLQLAEKNGYVTVSEIKASLKWETERARQVLEHLLKEGLAWLDLQAPGEAHYWLPALF  240

C. elegans 244 LQQYCHSSSSTSVSESL                                            260
H. sapiens 241 TDLYSQEITAEEAREAL                                           257
```

Vps36

```
C. elegans 1   MNRLSWYTPG--ESTEELLCQAGHVGIYEGDLKQTNFEQGTASLTMQRIIWADSSDPDRR  58
H. sapiens 1   MDRFVW-TSGLLEINETLVIQQRGVRIYDGE-EKIKFDAGTLLLSTHRLIWRDQKNHECC  58

C. elegans 59  LVLHHSLVISMEKHHKSMFSKGGKIVVKLEK-PKAGNIGPVNSSHYETLRLVFRHGGEDD  117
H. sapiens 59  MAILLSQIVFIEEQAAGI-GKSAKIVVHLHPAPPNKEPGPFQSSKNSYIKLSFKEHGQIE  117

C. elegans 118 FFKKYEDAVRRKTWQRSSSGSSSSGSRASS--NLRSVGISGIERRLAENHQKTHETITQA  175
H. sapiens 118 FYRRLSEEMTQRRWENMPVSQSLQTNRGPQPGRIRAVGIVGIERKLEEKRKETDKNISEA  177

C. elegans 176 FDDMSKLMETAREMVALSKSISEKVRSRKGEISEDETIAFKSYLLSLGVSDPVTKSTFVG  235
H. sapiens 178 FEDLSKLMIKAKEMVELSKSIANKIKDKQGDITEDETIRFKSYLLSMGIANPVTRETY-G  236

C. elegans 236 SDSEYFQKLAKEISDVLYEHIKENGGMCALPEVYCRINRARGMELLSPEDVMNACGALSR  295
H. sapiens 237 SGTQYHMQLAKQLAGILQVPLEERGGIMSLTEVYCLVNRARGMELLSPEDLVNACKMLEA  296

C. elegans 296 INSPLELHRFPSGVLVVQLKSASMDSTVGQTLEFVSKLERASANELAESLGITVILARER  355
H. sapiens 297 LKLPLRLRVFDSGVMVIELQSHKEEEMVASALETVSEKGSLTSEEFAKLVGMSVLLAKER  356

C. elegans 356 LLAAEESGLICRDDSIEGLLFYPNRFM                                  382
H. sapiens 357 LLLAEKMGHLCRDDSVEGLRFYPNLFM                                 383
```

Vps20

```
C. elegans 1   MGGIFSKKEKSPKSAPVSDQDNAILALKTQRDKMKQMIKRKENCLEKERQLAKQLIKDGR  60
H. sapiens 1   MGNLFGRK----KQSRVTEQDKAILQLKQQRDKLRQYQKRIAQQLERERALARQLLRDGR  56

C. elegans 61  KDRALLLLKKKRYQEKIIDQTLNHLSKIEQMVNDLEFAEVQQRVTDGLRQGNEALKKMNQ  120
H. sapiens 57  KERAKLLLKKKRYQEQLLDRTENQISSLEAMVQSIEFTQIEMKVMEGLQFGNECLNKMHQ  116

C. elegans 121 LFDIDEIDRIMEETKEAAEYQEEISNMLSGQLSNTDVSDVEKELEDLLAAEWGTVQLPEA  180
H. sapiens 117 VMSIEEVERILDETQEAVEYQRQIDELLAGSFTQEDEDAI---LEELSAITQEQIELPEV  173

C. elegans 181 PSHELPEAERERQKEKEKPRREKIA                                     205
H. sapiens 174 PSEPLPEKIPENVPVKARPRQAELV                                    198
```

Vps32

```
C. elegans 1   MSLFGKIFGGRKQEAPS---TPQESIQKLRETEEMLEKKQEFLEKKVIDEKQNAVKYGTK  57
H. sapiens 1   MSVFGKLFGAGGGKAGKGGPTPQEAIQRLRDTEEMLSKKQEFLEKKIEQELTAAKKHGTK  60

C. elegans 58  NKRMALQCLNRKRNFEKQLAHIDGVLSTIGYQREALENASTNAEVLNVMGTASKALKAAH  117
H. sapiens 61  NKRAALQALKRKKRYEKQLAQIDGTLSTIEFQREALENANTNTEVLKNMGYAAKAMKAAH  120

C. elegans 118 NNMDIDQVHDLMEDIAEQQEVANEIAEAISNPVGFSTAVDDDDLMRELEALEQEELDKEL  177
H. sapiens 121 DNMDIDKVDELMQDIADQQELAEEISTAISKPVGFGEEFDEDELMAELEELEQEELDKNL  180

C. elegans 178 LDARAP-PVTLPDTPNIALPAVPASRPRAKEADKDLEDLESWANA                 221
H. sapiens 181 LEISGPETVPLPNVPSIALPSKPAK--KKEEEDDDMKELENWAGS                 223
```

D

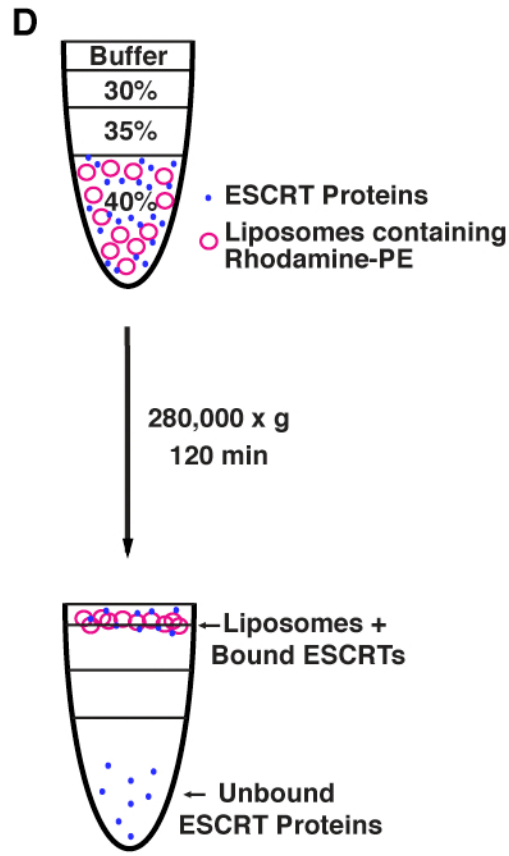

Fyfe et al., Figure S1

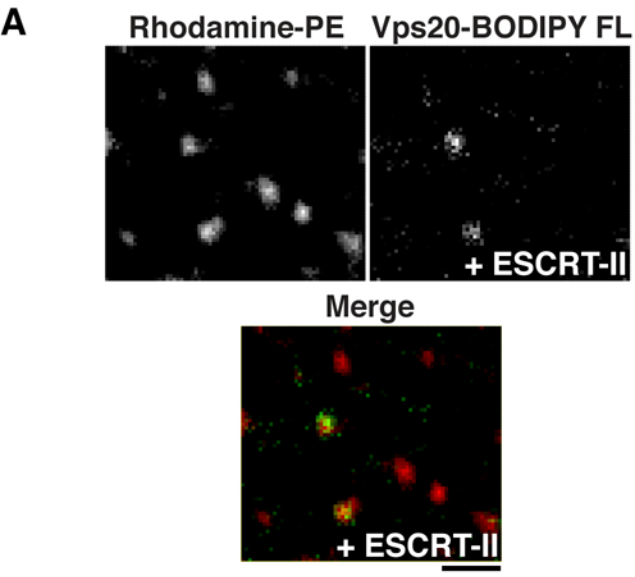

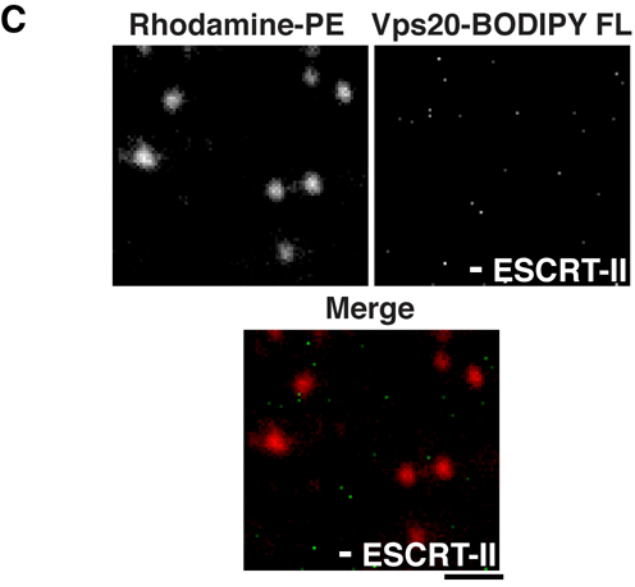

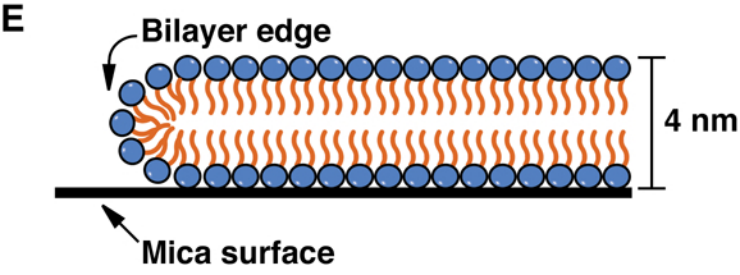

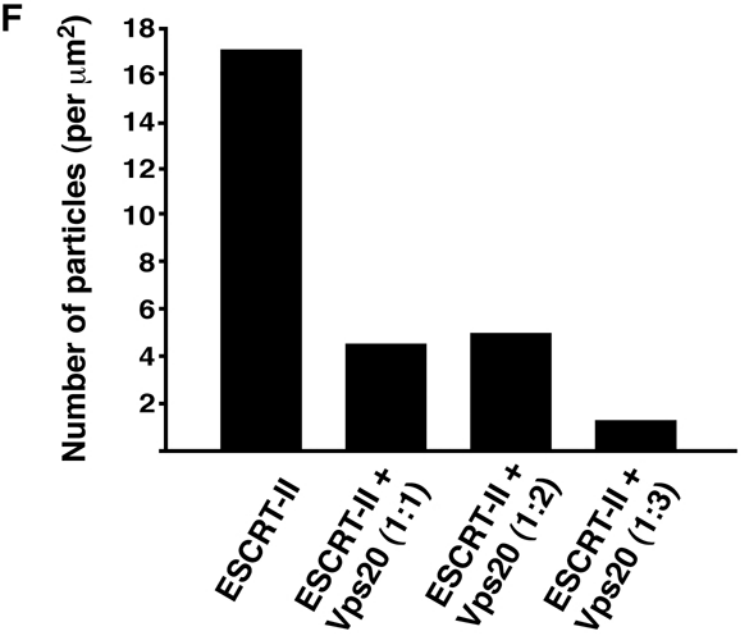

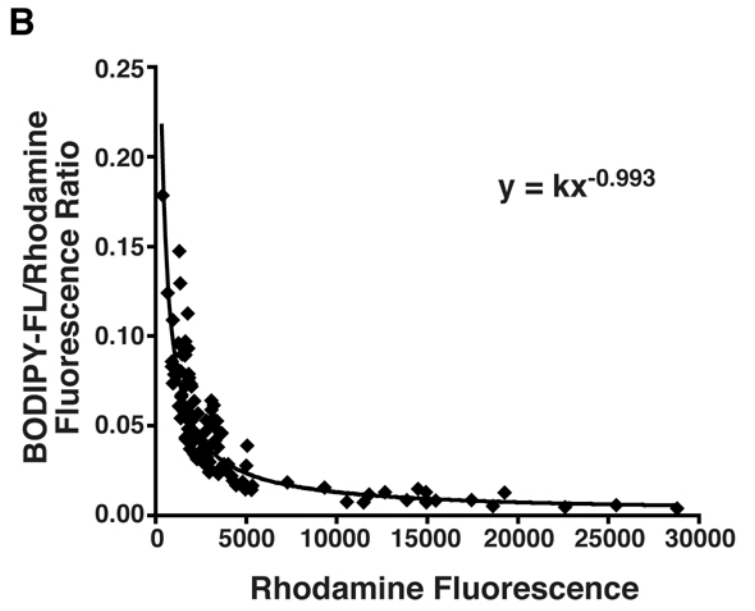

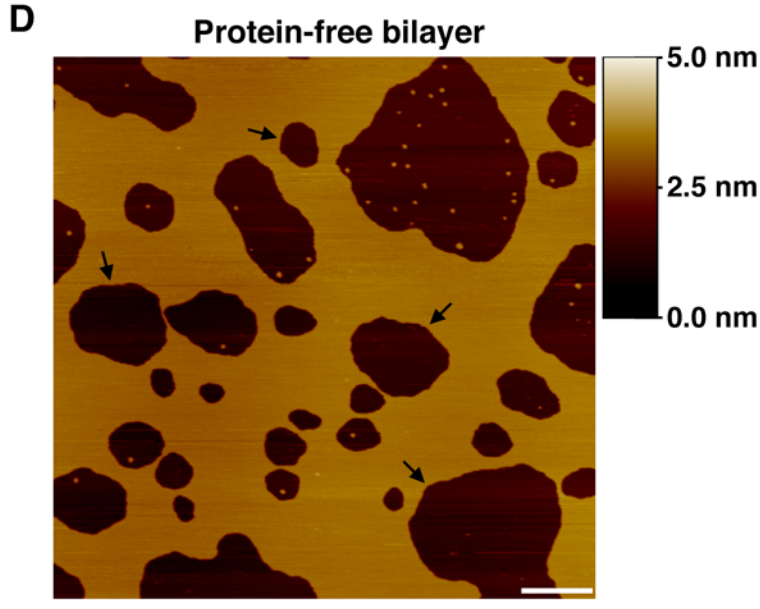

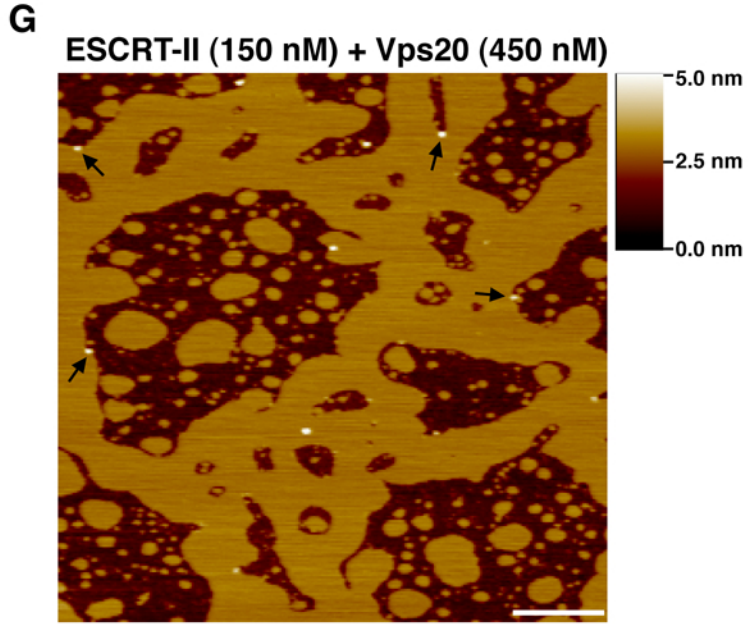

Fyfe et al., Figure S2

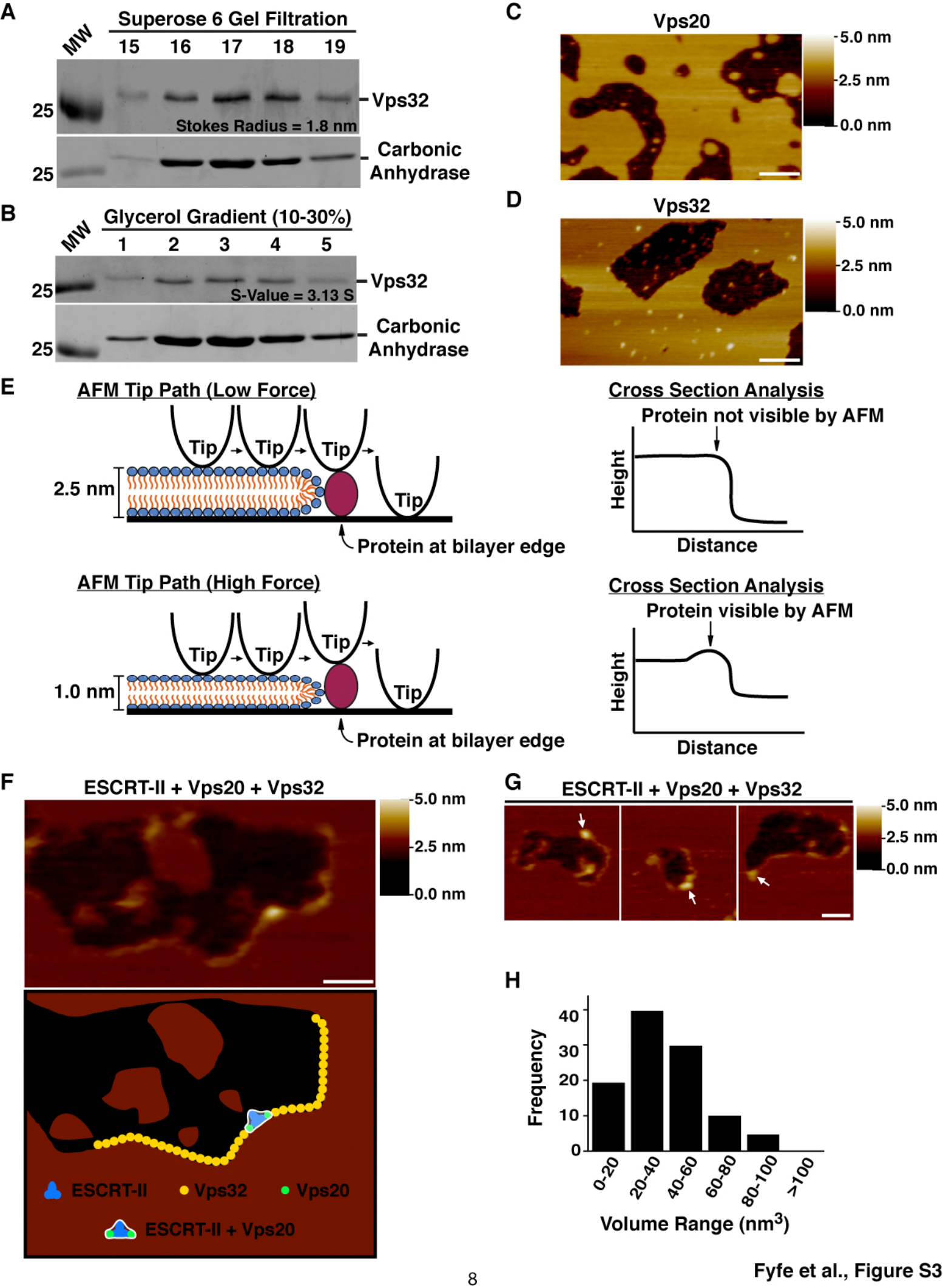

Fyfe et al., Figure S3

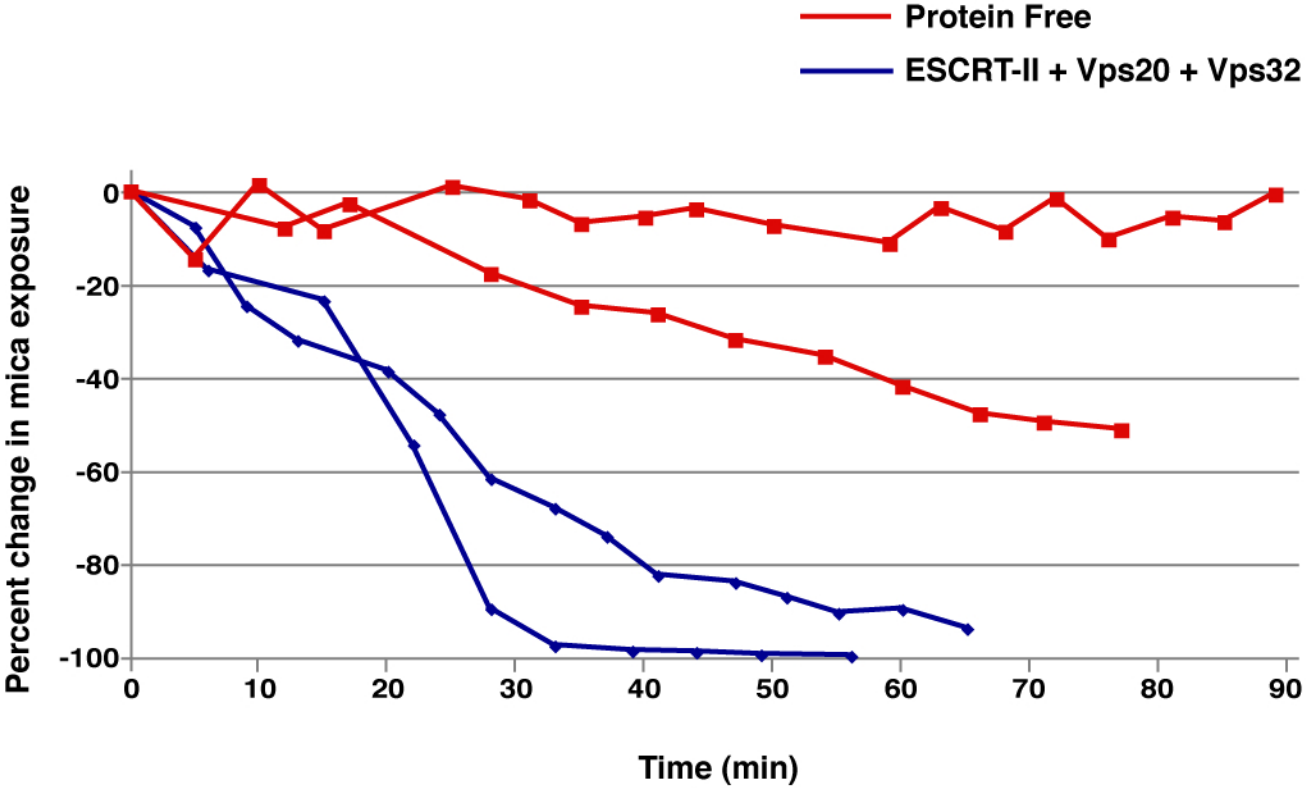

Fyfe et al., Figure S4